

Geophysical Research Letters

Supporting Information for

**Rupture process of the Mw=7.9 2015 Gorkha earthquake (Nepal):
insights into Himalayan megathrust segmentation**

Grandin Raphaël¹, Vallée Martin¹, Satriano Claudio¹, Lacassin Robin¹, Klinger Yann¹,
Simoes Martine¹, Bollinger Laurent²

¹ Institut de Physique du Globe de Paris, Sorbonne Paris Cité, Univ Paris Diderot, CNRS, F-75005 Paris, France,

² CEA, DAM, DIF, Arpajon, France

Contents of this file

Figures S1 to S9

Tables S1 to S2

Data Sets S1 to S4

Introduction

This supporting information provides additional figures showing in more details the back projection results (Figures S1 and S2), the interseismic coupling data set and model (Figures S3 and S4), the evolution of slip deduced from the kinematic inversion (Figure S5), the results of a supplemental inversion test showing the robustness of the source model with respect to smoothing constraints (Figures S6 and S7), the static inversion for the 12 May 2015 aftershock (Figure S8), and the broadband waveform agreement between synthetics and data at station KKN4 (Figure S9).

Additional tables also list the SAR acquisitions (Table S1) and the velocity model (Table S2) used in this study.

Data sets include slip parameters for the 25 April 2015 mainshock deduced from the kinematic inversion (Data Set S1), space-time evolution of back-projection peaks (Data Set S2), slip distribution for the 12 May 2015 aftershock computed from the static inversion (Data Set S3) and spatial distribution of interseismic coupling (Data Set S4).

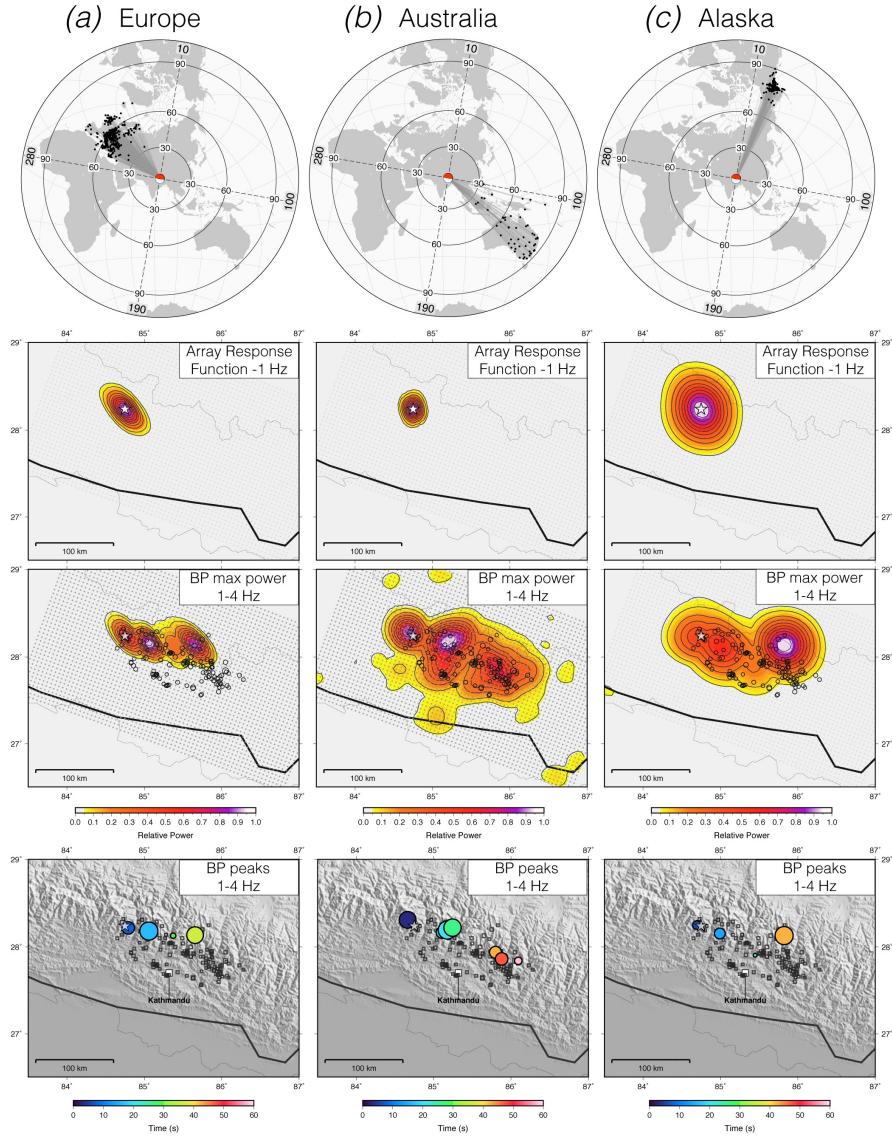


Figure S1. Back projection (BP) analysis from stations in Europe (*left column*), Australia/Southeast Asia (*center column*) and Alaska (*right column*). *Top line*: station distribution. *Second line*: Array response function (ARF), computed from BP of a point source located at the epicenter (white star) and emitting a monochromatic 1Hz signal. Gray dots indicate the search grid nodes; grid size is 350 km x 200 km; grid spacing is 5 km. The size of the ARF indicates the theoretical resolution and is mainly controlled by the array aperture [Xu et al., 2009]. *Third line*: normalized maximum BP power over time from semblance-weighted linear stack in the 1-4 Hz frequency band. Black circles are aftershocks, up to May 4, located by NSC. These images are controlled by the array aperture, which determines the resolution (see the ARF above), and by the station density. The Australian network, which is sparser, produces a more scattered image. *Bottom line*: BP peaks colored by elapsed time and scaled by normalized BP power. Peaks are extracted as local maxima of BP power in space and time, taking into account the array response function. Only peaks with normalized BP power larger than 0.2 are considered.

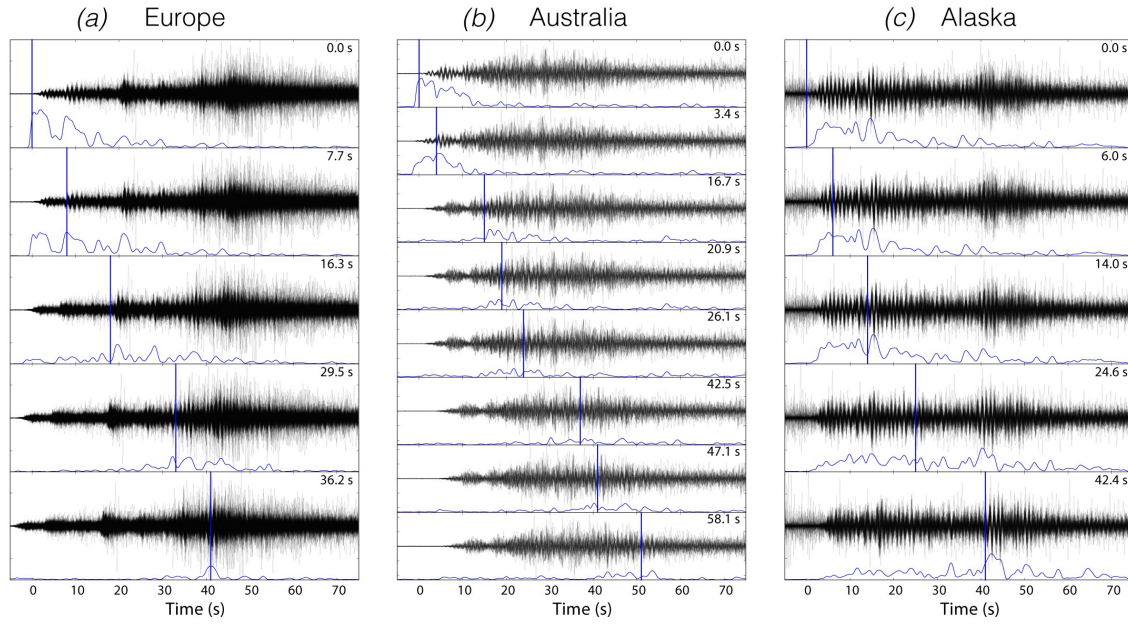


Figure S2. Trace alignment for back projection (BP) peaks. (a) normalized and superimposed velocity records (1.0 - 4.0 Hz) at the European stations, aligned according to the travel time from the hypocenter (topmost plot) or from the detected BP peaks. BP peak time is indicated, for each plot, by the label in the upper right corner. The blue curve is trace semblance, indicating waveform coherency. (b and c) same as (a), but for Australian/Southeast Asian stations and Alaska stations, respectively. For the Alaska traces, the high signal level before the first P arrival is due to a ML4.7 earthquake in Southern Alaska.

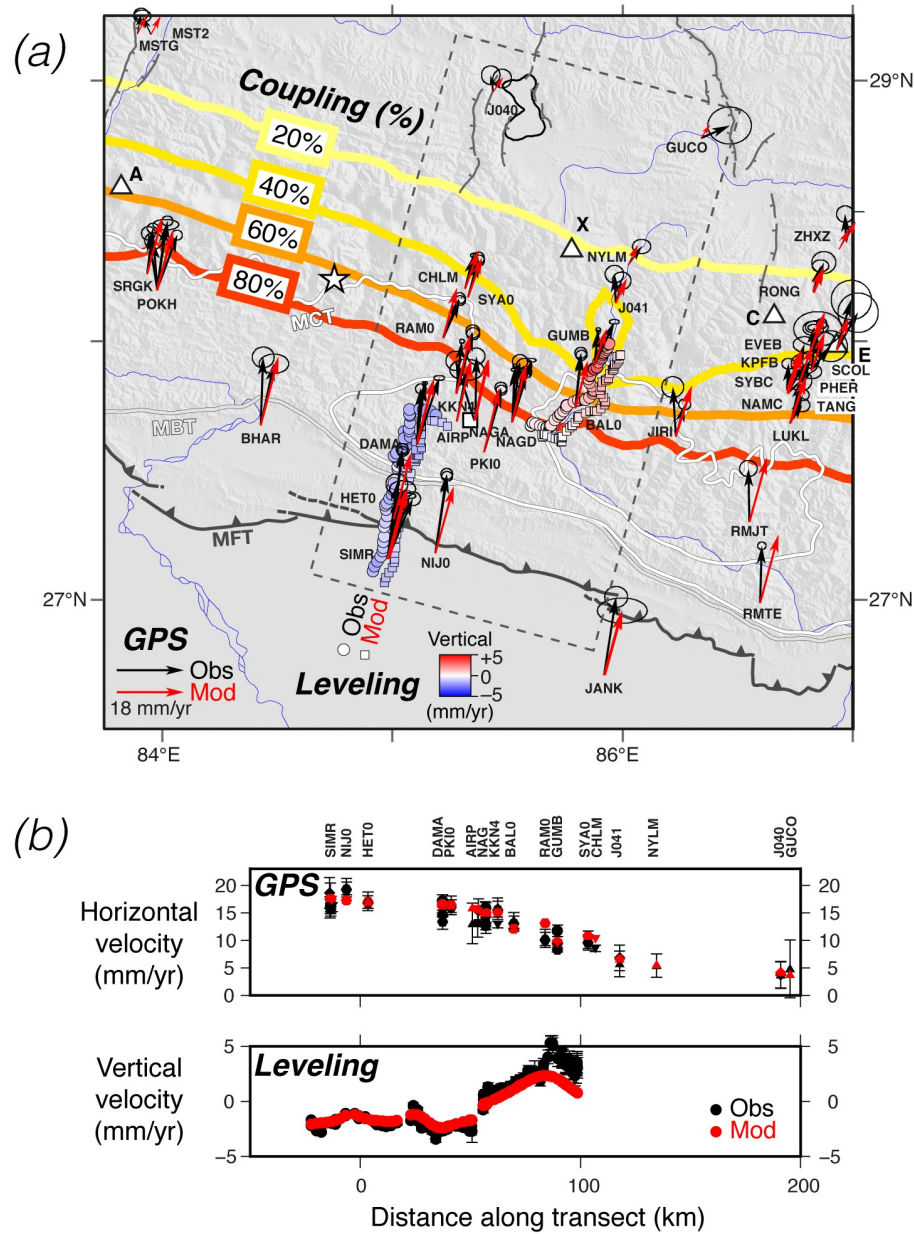


Figure S3. Interseismic coupling model. (a) Observed (black) and modeled (red) GPS velocity vectors from a compilation of continuous and campaign GPS data [Bettinelli et al., 2006; Feldl and Bilham, 2006; Socquet et al., 2006; Gan et al., 2007; Banerjee et al., 2008; Ader et al., 2012]. Tibet plateau is the reference for the GPS velocities. Convergence rate is fixed to 18 mm/yr and convergence azimuth is fixed to N10°E. The leveling profile of Jackson and Bilham [1994] is also included, with the circles and squares corresponding respectively to observed and modeled vertical velocities. The thick colored lines represent contours of the coupling gradient percentage. (b) Horizontal velocities (top) and vertical velocities (bottom) along a transect perpendicular to the Himalaya shown by the dashed box in (a).

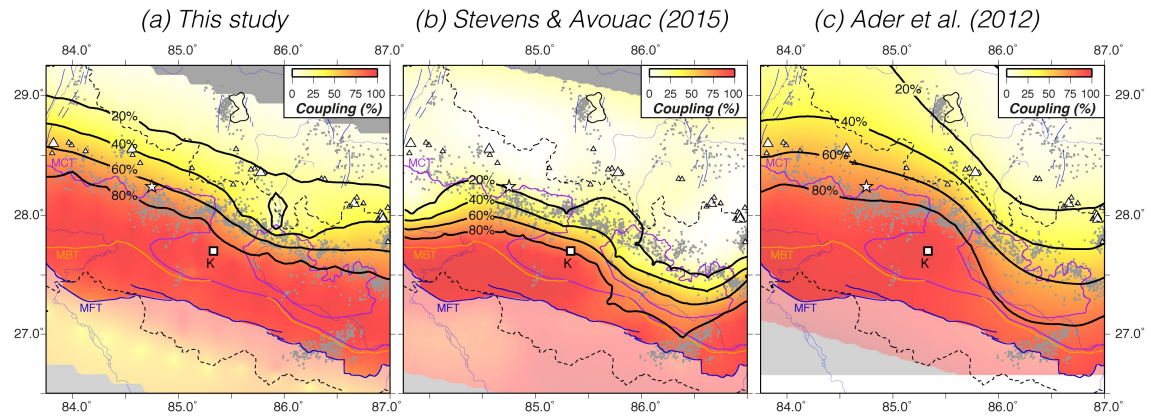


Figure S4. Comparison of interseismic coupling models in the area. (a) This study. See also Figure 4 and S3. (b) Stevens and Avouac [2015]. (c) Ader et al. [2012]. Grey dots show the background seismicity from NSC. White star is the hypocenter of the 25 April 2015 earthquake reported by NSC. The dashed black lines show the international borders. Reference : Stevens, V. L., & Avouac, J. P. (2015). Interseismic coupling on the main Himalayan thrust. *Geophysical Research Letters*, 42(14), 5828-5837.

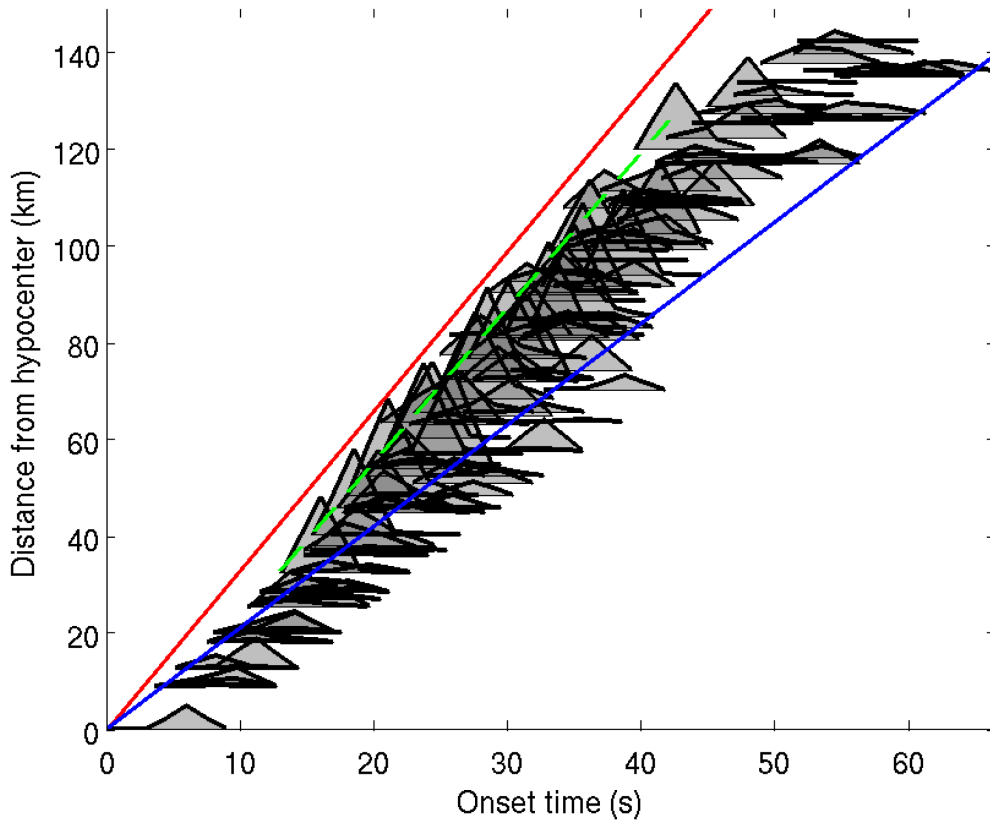


Figure S5. Time-distance plot of the moment release during the Gorkha earthquake. The local source functions (LSTFs) of each point of the fault (parametrized by 2 overlapping triangles with a duration of 6 s) are shown on the figure. Each LSTF is located by its scalar distance to the hypocenter (vertical scale). On the horizontal scale, the LSTFs are shown with respect to the rupture initiation time. Their onset time was allowed to vary between the blue and red lines (corresponding to rupture velocities of 2.1 km/s and 3.3 km/s, respectively). During the main moment release of the earthquake (between 15s and 40s after origin time), the rupture velocity is almost constant, as illustrated by the dashed green line corresponding to a rupture velocity of 3.2km/s.

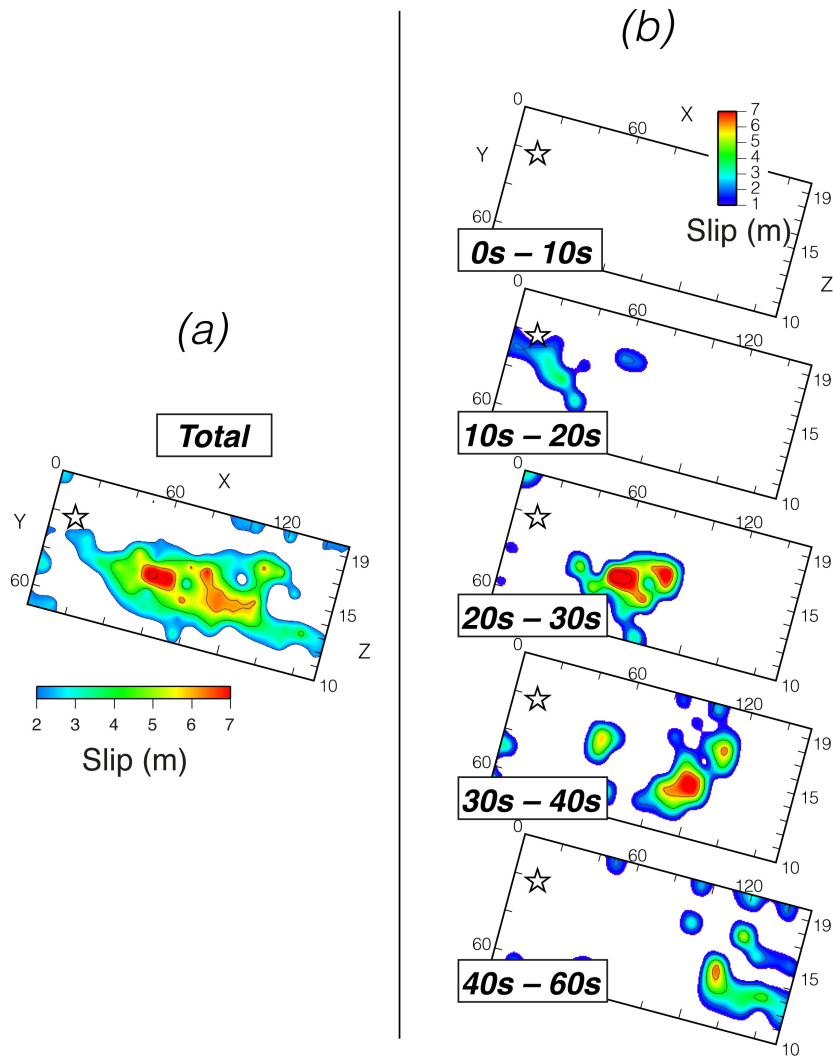


Figure S6. Source process retrieved from the inversion test where (1) slip and rupture velocity smoothing constraints are fully relaxed and (2) permitted rupture velocity range is larger. a) Final slip distribution with 2m slip contours (to be compared with Figure 2a) b) Snapshots of slip distribution as a function of time deduced from kinematic inversion (to be compared with Figure 2b). The features of the source process discussed in the study (rupture extension along-strike and along-dip, average slip inside the main patch, eastward rupture progression at $\sim 3.2\text{km/s}$) still appear clearly in this much less constrained inversion. Compared with the preferred model shown in Figure 2, the differences are a higher peak slip (reaching 9m), the presence of some residual slip close to the borders of the fault, and some points with delayed slip (see also Figure S7), but carrying a small percentage of the global moment. None of these second-order characteristics are required as the global fit cannot be distinguished from the fit of the inversion shown in the main text.

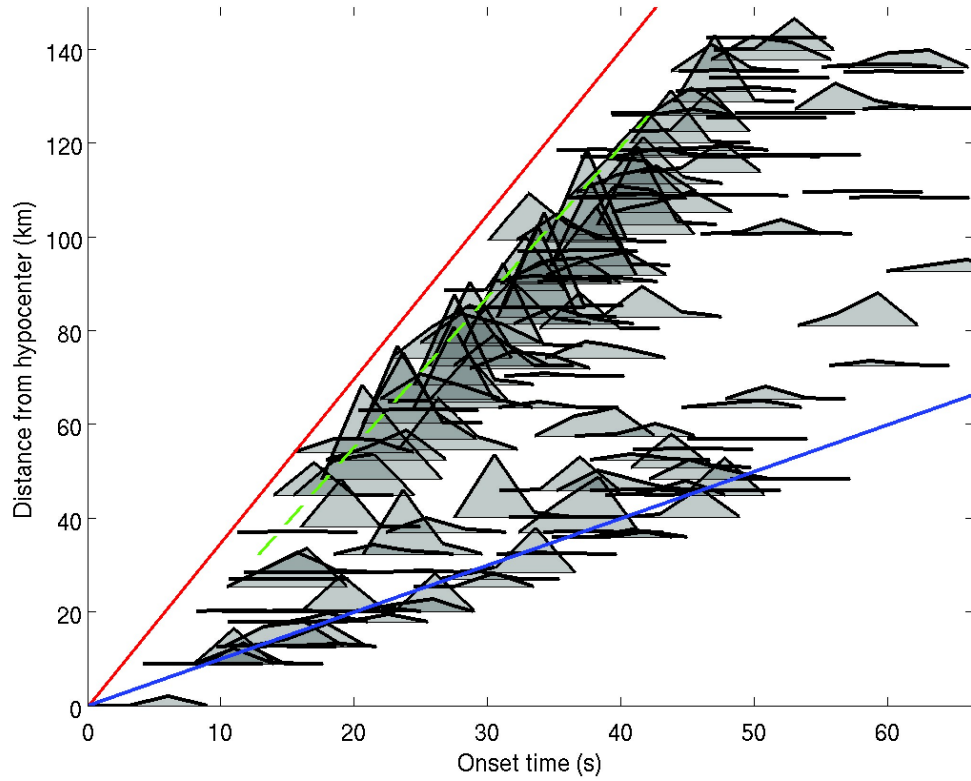
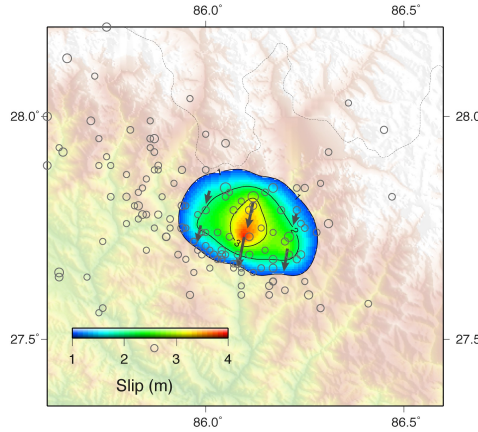


Figure S7. Same as figure S5, but for the inversion test where (1) slip and rupture velocity smoothing constraints are fully relaxed and (2) permitted rupture velocity range is larger. The onset times of the LSTFs are still allowed to vary between the blue and red lines, which now correspond to rupture velocities of 1 km/s and 3.5 km/s, respectively. Even if the inversion is much more free in this case, the same features of the rupture propagation are observed: most of the seismic moment is released along the dashed green line, which corresponds to a rupture velocity of 3.2 km/s. The delayed slip, mostly observed along the 1km/s blue line, represents only a small fraction of the total moment release and therefore does not significantly improve the data agreement.

Gorkha earthquake
12 May 2015 Aftershock
(Mw7.3)

(a) Slip model



(b) InSAR

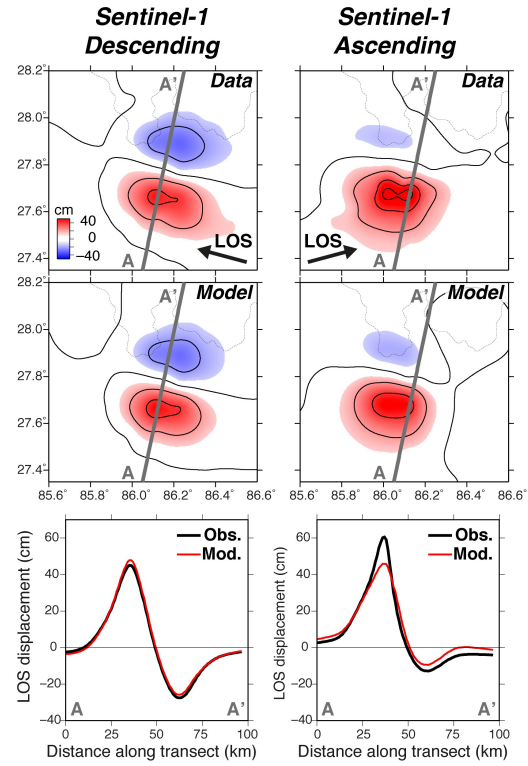


Figure S8. Slip model for the 12 May 2015 aftershock (Mw7.3) deduced from Sentinel-1 InSAR data. (a) Distribution of slip at depth. The centroid is located at approximately 15 km. Grey circles are aftershocks reported by NSC. (b) Observed (top) and modeled (middle) line-of-sight (LOS) displacement. The left and right panels are for descending and ascending geometries, respectively. The LOS vector is indicated by the black arrow. Red (positive) corresponds to motion towards the satellite, whereas blue (negative) corresponds to motion away from the satellite. The bottom panels show LOS displacements along the transect A-A' indicated in upper panels.

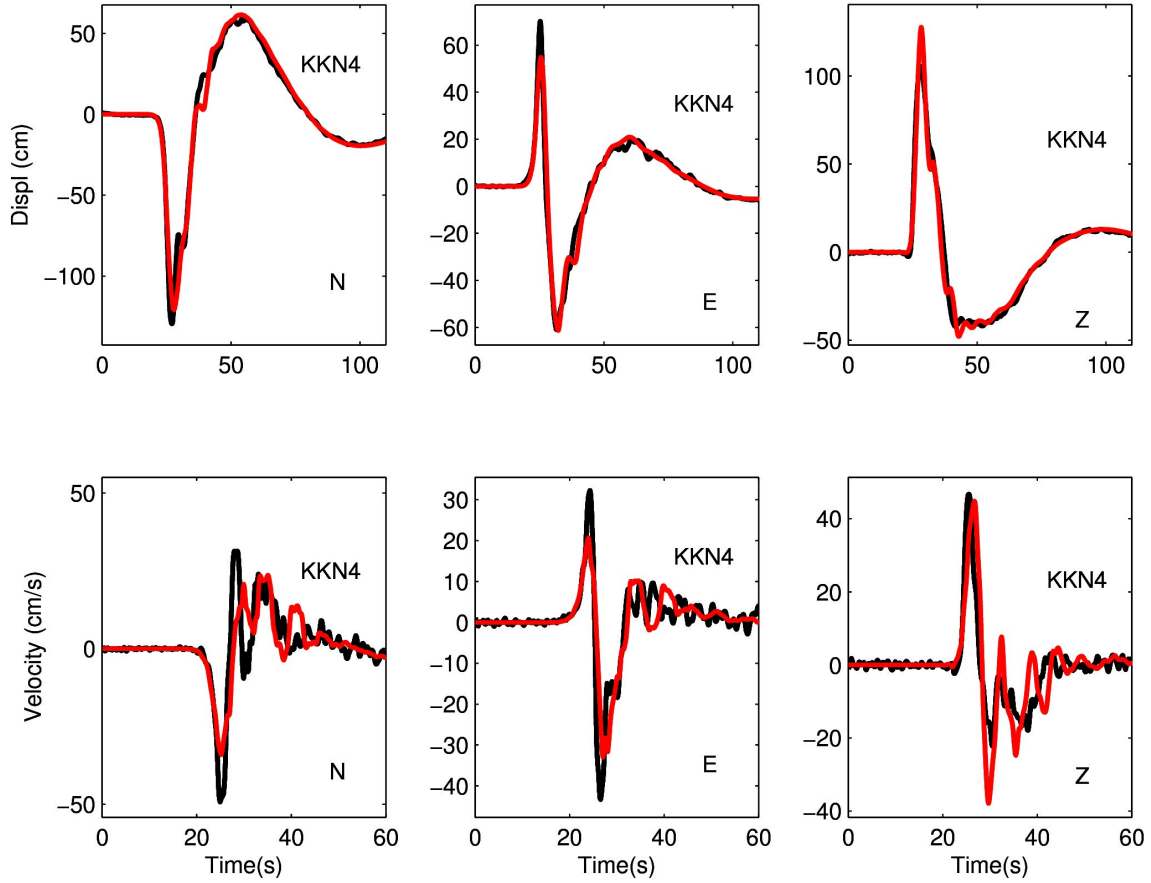


Figure S9. Data agreement observed at high-rate GPS station KKN4 in the [0.01Hz-1Hz] range. Data are in black and synthetics corresponding to the source model shown in Figure 2 are in red. The 3 components (North, East, vertical) of the displacements are shown in the top row and the 3 components (North, East, vertical) of the velocities in the bottom row. The model inferred from our inversion is in excellent agreement with the displacement records up to frequencies much higher than the ones included in the inversion (1Hz compared to 0.1Hz), thus confirming the reality of the smoothness of the source process. Note that even the velocity records, where the high frequency content is enhanced, are well modelled. Such a simple comparison cannot be done at stations inside Kathmandu (KATNP and NAST) because of strong basin effects at periods around 4s [Goda et al., 2015 ; Galetzka et al., 2015], that cannot be modeled with the simple 1D crustal structure shown in Table S2.

Table S1. List of SAR acquisitions used in this study.

25/04/2015 – Mainshock (Mw7.9)			
Platform	Geometry	Master	Slave
Sentinel-1	Ascending	21/04/2015	03/05/2015
Sentinel-1	Descending	17/04/2015	29/04/2015
Sentinel-1	Ascending	09/04/2015	03/05/2015
Sentinel-1	Descending	12/04/2015	06/05/2015
Sentinel-1	Descending	24/04/2015	06/05/2015
ALOS-2	Ascending	22/02/2015	03/05/2015
ALOS-2	Ascending	21/02/2015	02/05/2015
12/05/2015 – Aftershock (Mw7.3)			
Platform	Geometry	Master	Slave
Sentinel-1	Ascending	03/05/2015	15/05/2015
Sentinel-1	Descending	06/05/2015	18/05/2015
ALOS-2	Descending	03/05/2015	17/05/2015

Table S2. Velocity model.

Layer	Top depth (km)	Bottom depth (km)	V_p (km/s)	V_s (km/s)	Density (g/cm ³)	Q_p	Q_s
1	0	6	5.60	3.23	2.46	500	200
2	6	12	6.30	3.64	2.70	500	200
3	12	18	6.40	3.70	2.74	500	200
4	18	24	6.50	3.75	2.77	500	200
5	24	30	6.60	3.81	2.81	500	200
6	30	36	6.70	3.87	2.84	500	200
7	36	42	6.80	3.93	2.88	500	200
8	42	48	6.90	3.98	2.91	500	200
9	48	–	8.00	4.62	3.30	1000	500

Data Set S1. Kinematic slip model for the 25 April 2015 mainshock.

Data Set S2. Space-time location of back-projection peaks.

Data Set S3. Static slip model for the 16 May 2015 aftershock.

Data Set S4. Interseismic coupling model.